Classification of slag material by spectral induced polarization laboratory and field measurements

Martin, Tina; Günther, Thomas; Weller, Andreas; Kuhn, Kerstin

Published in:
Journal of Applied Geophysics

DOI:
10.1016/j.jappgeo.2021.104439

2021

Document Version:
Publisher's PDF, also known as Version of record

Journal of Applied Geophysics 194 (2021) 104439

Contents lists available at ScienceDirect

Journal of Applied Geophysics

journal homepage: www.elsevier.com/locate/jappgeo

Classification of slag material by spectral induced polarization laboratory and field measurements

Tina Martin [a,b,*], Thomas Günther [c], Andreas Weller [d], Kerstin Kuhn [b]

[a] Engineering Geology, Lund University (LU), John Ericssons väg 1, SE-22363 Lund, Sweden
[b] Federal Institute for Geosciences and Natural Resources (BGR), Stilleweg 2, D-30655 Hannover, Germany
[c] Leibniz Institute for Applied Geophysics (LIAG), Stilleweg 2, D-30655 Hannover, Germany
[d] Clausthal University of Technology, Institute of Geophysics, Arnold-Sommerfeld-Straße 1, D-38678 Clausthal-Zellerfeld, Germany

ARTICLE INFO

Keywords:
Frequency domain
Complex electrical conductivity
Spectral inversion
Slag dumps
Harz Mountains
Economic potential

ABSTRACT

Historical slag dumps are of increasing interest due to economic, environmental or archaeological reasons. Geophysical investigations can help accessing the potential reuse of slag material to recover metallic raw material or for the estimation of the hazard potential of the buried slag material due to dissolution occurrence.

In our study, we have investigated various slag material in the laboratory with the spectral induced polarization (SIP) method, obtained from different historical slag dumps, located in the Harz Mountains, Germany. We also present SIP results from field measurements at a historical slag dump where most of the slag samples reveal high amounts of iron, zinc, silica, and barium.

Our results reveal a discrimination between three different slag grades (low, medium, high) by using the imaginary conductivity σ'' at a medium frequency (1–10 Hz) in both laboratory and field. Furthermore, additional information is obtained by a classification based on the spectral polarization behaviour and considering the field frequency range (0.1 Hz – 100 Hz). Five different types of spectra (ascending, descending, constant, maximum and minimum type) can be discriminated and recognized in the laboratory and in distinct areas of the slag dump. Even though a direct comparison between the laboratory and field results still needs to be proven, the buried slag material can be differentiated from the surrounding material by the polarization magnitude.

1. Introduction

Decreasing ore grades within deposits, the increasing demand for raw materials and volatile prices due to political influence on the markets, have raised awareness to the diversification of supply. One potential important source to meet the needs can be to recover raw materials from mining waste (Kuhn and Meima, 2019). Due to former no-need or inefficient ore processing in the past, many old mining waste sites in the Harz Mountains, Germany, still contain high metal contents, which might be worthwhile to explore. Although, an overall assessment of the economic value of these dumps is often difficult to conduct since there are many factors other than the metal content that influence the value. For example, due to the presence of heavy metal contents, mine waste does not only represent a stock of valuable raw materials but has also a considerable risk for the contamination of groundwater, surface water, soils, and sediments. Hence, the costs for remediating mine waste bodies must be included in cost-benefit considerations.

The aim of the geophysical investigations was now to investigate the internal structure of the dumps and to characterize and possibly classify residual slag material to enable an estimation of valuable recycling material.

Over the past few years, various geophysical investigations using the spectral induced polarization (SIP) method at historical mining dumps or tailings have been conducted for archaeological or environmental reasons (e.g., Weller et al., 2000; Ullrich et al., 2007; Placencia-Gomez et al., 2010, 2015; Florsch et al., 2011, 2012, 2017; Martin et al., 2020b). Additionally, laboratory measurements have shown the high sensitivity of the SIP method to metal sulphides (e.g., Placencia-Gomez et al., 2013; Hupfer et al., 2016). It is also known that the concentration and mineral grain sizes of different minerals can be estimated by SIP using parameter derived from IP measurements (Pelton et al., 1978; Florsch et al., 2011; Hupfer et al., 2016; Qi et al., 2018).

Nowadays, due to recent two-dimensional inversion algorithm (Günther and Martin, 2016) and new approaches to detect and quantify

* Corresponding author at: Engineering Geology, Lund University (LU), John Ericssons väg 1, SE-22363 Lund, Sweden.
E-mail address: tina.martin@tg.lth.se (T. Martin).

https://doi.org/10.1016/j.jappgeo.2021.104439
Received 14 October 2020; Received in revised form 17 June 2021; Accepted 18 August 2021
Available online 20 August 2021

buried slags (Qi et al., 2018), the analysis of the field SIP data at slag dumps has been significantly improved. Accordingly, it is possible to improve the interpretation of the residual mineral content such that spatial information about the mineral content of historical dumps can be assessed.

In this study, we present results from SIP laboratory measurements at various slag, ore, and country rock material such as clay shale, greywacke and claystone. The slags are remains from the pyrometallurgical treatment of ores from the Rammelsberg deposit (zinc, lead, copper, and silver) or the vein deposit of the Upper Harz (lead, zinc, silver, minor copper).

We identified varying spectral behaviour for the different materials. Only few samples display a so-called Cole-Cole type with an accentuated maximum in the spectrum of the imaginary part of conductivity (e.g., Cole and Cole, 1941; Pelton et al., 1978, 1983; Tarasov and Titov, 2013). Instead of a maximum, some samples indicate a continuous increase or decrease of the imaginary part of conductivity as function of frequency. Other samples display constant phase angle spectra in the measured frequency range (e.g., Dissado and Hill, 1984; Börner et al., 1996). This diversity of spectral behaviour does not allow a fitting of all spectra by a single model. The use of the Cole-Cole model as universal model as assumed in a variety of studies (e.g., Yoshioka and Zhdanov, 2005; Loke et al., 2006; Fiandaca et al., 2012; Günther and Martin, 2016; Johansson et al., 2020) would ignore the diversity of spectral behaviour as revealed in laboratory investigation on slag material.

Therefore, we propose a type classification of the different material based on their spectral polarization behaviour, which is identified by laboratory measurements. Two field SIP profiles were investigated at the dump Kanstein, a copper smelter from the Middle Ages to the Late Middle Ages. The full set of multi-frequency 2D field data have been inverted by an algorithm with a smoothness-constraint applied to adjacent frequencies (Günther and Martin, 2016). We apply our classification to the resulting field spectrum of each subsurface element. Using the type classification, the resulting depth sections enable a zonation of the dumps in areas with different slag material.

2. Method and material

2.1. Spectral induced polarization method

The Induced Polarization (IP) method investigates both electrical conduction and polarization phenomena of rocks and other material as (e.g.,) wood, through laboratory and field measurements applied in the time or in the frequency domain. In our study, we use frequency domain measurements in a frequency range. This method is referred to as spectral induced polarization (SIP). A SIP survey is performed by an impedance spectrometer that registers the amplitude of impedance and the phase shift between injected sinusoidal current signal and measured voltage. The resulting impedance Z is a complex frequency dependent quantity:

$$Z(\omega) = |Z(\omega)|exp(-i\varphi(\omega)) \quad (1)$$

with $\omega = 2\pi f$ being the angular frequency, $i = \sqrt{-1}$ the imaginary unit, and $\varphi(\omega)$ the spectrum of the phase shift. The multiplication of the complex impedance by a geometric factor K yields a complex resistivity $\varrho^*(\omega)$. A conventional resistivity considers only the resistivity amplitude at a fixed frequency. We prefer to use the electrical conductivity, which is the inverse of resistivity, throughout our study, since the imaginary conductivity σ'' is closely related to polarization effects. The complex electrical conductivity σ^* results from the impedance measurement in a straightforward way:

$$\sigma^*(\omega) = \frac{exp(i\varphi(\omega))}{K|Z(\omega)|} = \sigma'(\omega) + i\sigma''(\omega), \quad (2)$$

where σ' and σ'' represent the real and imaginary part of electrical conductivity. The spectrum $\sigma'(\omega)$ describes the frequency dependence of electrical conduction that generally shows a continuous increase of conductivity with increasing frequency. The spectrum $\sigma''(\omega)$ describes the polarization phenomena as a function of frequency. The shape of the spectra $\sigma''(\omega)$ displays a wide variability for different material. Many studies are focused on the extraction of the spectral information from complex conductivity spectra $\sigma'(\omega)$ and $\sigma''(\omega)$. A variety of mathematical models has been designed to fit the measured spectra such as the Cole-Cole model with its four parameters high frequency conductivity σ_∞, chargeability m, time constant τ, and the Cole-Cole exponent c (Cole and Cole, 1941; Tarasov and Titov, 2013). We found that the Cole-Cole model could not reliably fit most of our measured spectra. A Debye decomposition can be an alternative approach (e.g., Nordsiek and Weller, 2008). Although the Debye decomposition enables a good fitting quality of arbitrary complex conductivity spectra, the number of unknown parameters increases. However, the interpretation of the resulting parameters in relation to the petrophysical properties of the samples remains challenging.

We propose in this this study a simpler approach that considers the main spectral features of $\sigma''(\omega)$. Considering the reduced frequency range of the field measurements, we applied a differentiation only between five types of spectra.

Several studies have demonstrated that the imaginary part of conductivity σ'', which corresponds to the polarization magnitude, is proportional to the normalized chargeability $m_n = \sigma_\infty - \sigma_0$ (e.g., Weller et al., 2010), where σ_∞ is the high frequency conductivity and σ_0 the low frequency conductivity. The normalization of the chargeability m by multiplying with the high-frequency conductivity σ_∞ is similar to the calculation of the metal factor from measurements of the frequency effect used in mineral exploration for evaluation the metal content of ores (Lesmes and Frye, 2001). Therefore, the quantity σ'' is a suitable parameter to assess the metal content of ores and slag. We use σ'' for a differentiation of the slag grade.

2.2. Investigation area

The Harz Mountains are located in the center of Germany (Fig. 1). Mining, processing and smelting of metal ores have been an important industrial sector in this area for more than thousand years, so there are still many heaps and dumps that provide evidence from mining, processing, and smelting activities at different historical periods. For the extraction of non-ferrous metals, the Rammelsberg massive sulphide deposit as well as hydrothermal vein deposits in different regions of the Harz Mountains were of particular importance. The Rammelsberg ore deposit is a world-class sediment-hosted massive sulphide deposit that was mined until 1988. Copper, lead, silver, and later also zinc and various trace metals, were extracted from more than 27 million tons of mined ore (Liessmann, 2010). Due to the small-sized and heavily intergrown minerals, the mechanical separation of the different ore minerals from each other and from the host rock was almost not possible until the introduction of the froth flotation process in the 1920s.

In contrast, silver ores, silver-rich lead ores, zinc ores and only sporadically copper ores were mined in the veins of the Upper Harz (Oberharz), a particularly ore-rich region (Sperling et al., 1981). The veins of the Upper Harz, which are up to 10 m thick, can be traced for up to 20 km and show particularly intensive mineralisation in areas where the veins split into a bundle of several individual veins (Liessmann, 2010). Approximately 37.9 million tonnes of raw ore were mined from the various deposits in the Upper Harz (Stedingk and Stoppel, 1993).

The slags examined in this study come from five different slag dumps and represent residues from the smelting of Rammelsberg ore or Upper Harz vein ore (Fig. 1, Table 1).

The two field profiles were gathered at the historical slag dump Kanstein, which is located at the northern margin of the Harz Mountains, where the estimated volume of the slag is around 100,000 m^3 (Kuhn et al., 2021). It contains slags from the pyrometallurgical treatment of

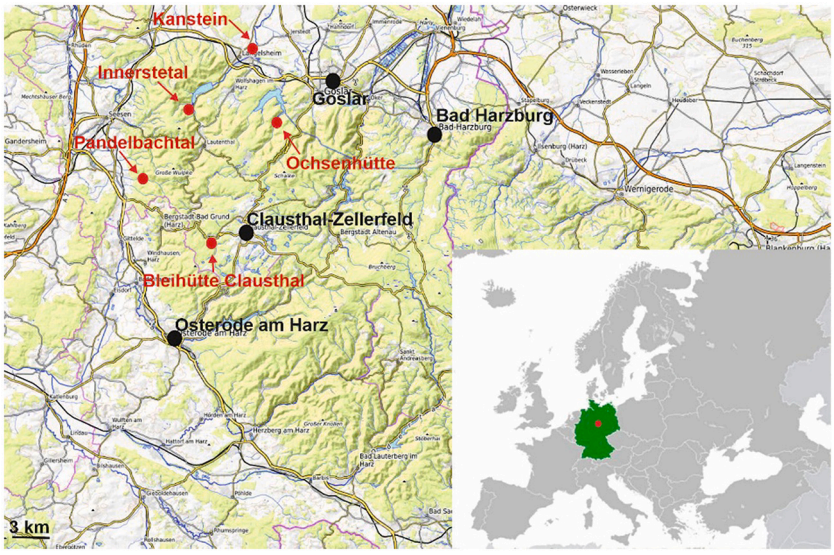

Fig. 1. Map of the Harz Mountains with major towns (black dots) and the locations of the slag sampling (red dots, see Table 1). Map source: Wikimedia, 2021 & OpenTopoMap, 2021. (For interpretation of the references to colour in this figure legend, the reader is referred to the web version of this article.)

Table 1
Overview about all investigated laboratory samples.

Material	Name	Location	Condition	Target metal	Origin of ore
Slag	**SO**	Ochsenhütte in the Granetal	solid	Cu	Rammelsberg
	SB	Bleihütte Clausthal	solid	Pb-Ag	Vein ore of Upper Harz
	SK 1	Kanstein	solid	Pb-Ag	Rammelsberg
	SK 2	Kanstein	solid	Pb-Ag	Rammelsberg
	KS 5	Kanstein	unconsolidated	Pb-Ag	Rammelsberg
	KS 6	Kanstein	unconsolidated	Pb-Ag	Rammelsberg
	KS 8	Kanstein	unconsolidated	Pb-Ag	Rammelsberg
	KS 9	Kanstein	unconsolidated	Pb-Ag	Rammelsberg
	XS-01-1	Pandelbachtal	solid	Cu	Rammelsberg
	XS-03-1	Pandelbachtal	solid	Cu	Rammelsberg
	XS-04-1	Pandelbachtal	solid	Cu	Rammelsberg
	XS-05-1	Pandelbachtal	solid	Cu	Rammelsberg
	XS-41	Innerstetal next to Innerstestausee	solid	Cu	Rammelsberg
Ore	**ZR01**	Goslar	solid	Cu	Rammelsberg
	ZR02	Goslar	solid	Cu	Rammelsberg
	ZR03	Goslar	solid	Cu	Rammelsberg
	ZR05	Goslar	solid	Cu	Rammelsberg
	ZE-01	Bad Grund	solid	Pb-Ag	Vein ore of Upper Harz
Country rock					
Clay shale	**ZR78A**	Goslar	solid	–	
Greywacke	**IFG-A01**	Clausthal	solid	–	
Greywacke	**IFG-A04**	Clausthal	solid	–	
Greywacke	**IFG-A07**	Clausthal	solid	–	
Claystone	**IFG-B07**	Clausthal	solid	–	
Claystone	**IFG-B11**	Clausthal	solid	–	
Claystone	**IFG-B12**	Clausthal	solid	–	

ore from the Rammelsberg deposit. The Kanstein smelter was active from the 13th century until the beginning of the 17th century and was renamed Herzog-Karl-Viktor smelter in the 16th century (Denecke, 1978; Sperling et al., 1981). However, the deposition of slags from other smelters (e.g., the nearby Frau-Sophien smelter, operation time: 1556–1941) cannot be excluded (Kuhn et al., 2021). Detailed information about the Kanstein dump with a focus on the geochemical investigation of the slag can be found in Kuhn et al. (2021).

2.3. Laboratory samples and instruments

For the laboratory investigations, different types of samples from various slag dumps in the Harz Mountains were collected (Figs. 1 and 2, left side). We investigated both, solid and unconsolidated slag material as well as original ore and country rock samples, also from the Harz Mountains. All slag samples were taken from the surface or in a maximum depth of 0.5 m. Details for the samples are compiled in Table 1. For some of the samples, geochemical and mineralogical analysis has been carried out. For the unconsolidated slag samples, only the grain size fraction <63 mm was examined, as the larger clasts were not used since they did not fit into the sample holder. Table 2 provides an overview about the main constituents. The investigated slags are rich in iron and silica (up to 54 wt.-% FeO + Fe_2O_3 and 30 wt.-% SiO2), with some samples also being enriched in CaO, Ba and Zn. Note that most of the iron in the slags occurs as FeO, but due to weathering processes, there are also phases that contain Fe_2O_3. During sample preparation, all FeO is converted into Fe_2O_3. Detailed laboratory results can be found in Kuhn et al. (2021).

Small drill cores for the SIP measurements were taken from each of the solid slag samples (Fig. 2, top left). The drill cores are 20 mm in

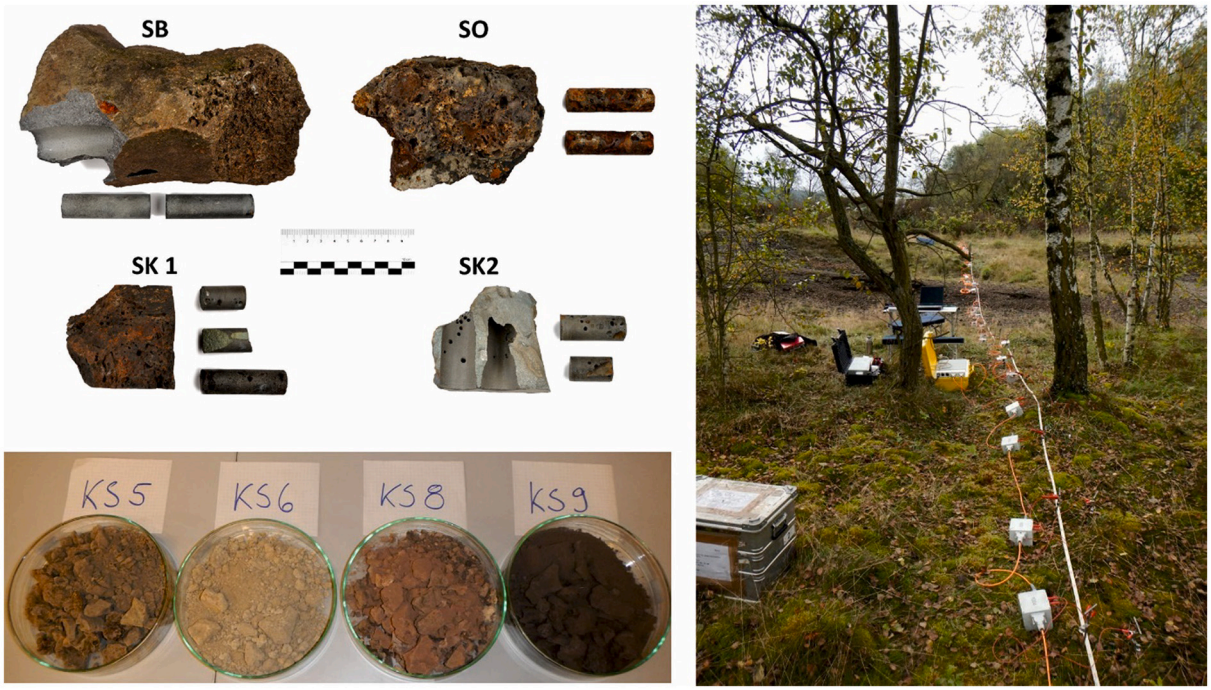

Fig. 2. Picture of selected samples from the slag dump Kanstein (left) and from the field Profile 1 (right) together with the used SIP 256C instrument (Radic Research).

Table 2
Overview about the bulk chemical composition of selected slag samples for the grain size fraction <63 mm (unconsolidated KS samples).

Sample	Ba [wt-%]	Pb [wt-%]	Zn [wt-%]	Cu [wt-%]	Fe_2O_3 [wt-%]	SiO_2 [wt-%]	CaO [wt-%]
SO	8.01	2.50	6.66	0.92	47.25	18.99	2.78
SB	2.80	2.73	2.23	0.05	39.63	30.49	17.51
SK 1	2.65	1.78	8.14	0.68	53.59	18.53	3.07
SK 2	3.80	3.83	8.57	0.51	43.55	25.30	4.26
KS 5	3.47	4.44	6.15	0.69	39.60	24.67	2.15
KS 6	3.59	5.67	2.33	0.26	30.25	31.04	2.03
KS 8	1.53	1.87	11.27	0.93	41.86	28.00	1.99
KS 9	12.17	3.28	14.33	1.29	29.96	15.11	1.88

diameter and vary in length between 30 mm and 70 mm. After cutting, the samples were saturated with and stored in tap water (conductivity of approx. 70 mS/m at room temperature). The unconsolidated bulk samples (Fig. 2, bottom left) with a volume of approx. 55 cm^3 were also saturated with tap water during the preparation in the sample holder.

For the laboratory SIP measurements, we used either the system ZEL-SIP04-V02 from *Forschungszentrum Juelich* (Zimmermann et al., 2008) with two amplifiers for the simultaneous measurement of two samples or the SIP Fuchs instrument from *Radic Research*. The latter one was used for samples collected in previous projects (ZR, ZE, and XS samples). The measurements were performed in a climate chamber to avoid temperature changes and to minimize electromagnetic noise due to it shielding behaviour (Faraday cage). We used two different sample holders. One was a four-point cell with ring wired potential electrodes made from German silver (Cu-Ni-Zn alloy). Here, the current electrodes consist of stainless steel and are placed at the end caps (see Kruschwitz, 2007). The second sample holder uses platinated platinum electrodes for current injection and rings of chloride silver wire surrounding the samples as voltage electrodes (see Schleifer et al., 2002).

Each sample was measured several times using the maximal frequency range of the equipment (e.g., 1 mHz and 45 kHz). Due to electromagnetic coupling effects at higher frequencies, we only show the laboratory SIP data until 1000 Hz.

2.4. Field measurements

Two SIP profiles were measured on the slag dump Kanstein with the SIP 256C instrument (*Radic Research*) and a varying number of remote units (Fig. 2, right side). The multi-channel, PC-controlled equipment records voltages for a current injection at different remote units in parallel. For all measurements, we applied the dipole-dipole array as it diminishes electromagnetic coupling between current and potential cables (Pelton et al., 1978). Fibreoptic cables were used for transferring the time series to the base unit. Due to the expected high IP signals, we used standard stainless-steel electrodes. Nevertheless, we attempted to minimize the electrode influence by using two electrodes at each measuring point: one for current injection (C) and the other for potential measurement (P). For the shown profiles, both electrodes (C/P) were at a distance of maximum 10 cm and inserted a few cm into the ground such to get sufficient coupling to the ground.

The two profiles had an electrode distance of 1 m but varied in length and frequency range. Profile 1 was 33 m long and inhomogeneously covered by a grass bed where moss and grass alternated with slags exposed to the surface (Fig. 2, right side). We measured at 13 frequencies between 0.3 Hz and 1000 Hz as it has been proven to obtain reliable data for the whole frequency range (Martin et al., 2020a). The topography along the profile was recorded and considered during inversion. The flat and grassy Profile 2 was 40 m long and recorded at 14 frequencies in a range between 0.16 Hz and 1000 Hz. A detailed description and inversion results for Profile 2 can be found in Günther and Martin (2016).

For the analysis of the measured data, we follow the numerical approach presented by Günther and Martin (2016), which is summarized here only briefly for completeness. It is based on the BERT inversion techniques (Günther et al., 2006) using finite element computations on irregular structured grids such that arbitrary topography can be included (Rücker et al., 2006). If every frequency is analysed individually, artefacts and ambiguity in the inversion results can hinder retrieving spectral subsurface information. The new method inverts all

data simultaneously with spectral constraints along the frequency axis in addition to spatial smoothness constraints (Günther and Martin, 2016). This algorithm ensures smooth spectra without pre-assuming a special behaviour such as the Cole-Cole model. As a result, we obtain a spectrum of the complex conductivity for every cell of the model discretization so that the spectral behaviour of different subsurface regions can be investigated.

2.5. Spectral classification

Due to the variety of different types of spectra for the slag material, we propose a classification system that is based on the spectral behaviour of σ″, rather than a Debye decomposition approach which results in an increased number of parameters. We define five different types to recognize and differentiate areas with slag and country rock material in the field frequency range (FFR) between 0.1 and 100 Hz. Consequently, in our analysis, we limit the laboratory frequency range to the FFR, and subdivided the frequency range into three parts (see also Fig. 3a):

I. a low frequency range (LF), between 0.1 and 1 Hz,
II. a medium frequency range (MF), between >1 and 10 Hz,
III. a high frequency range (HF), between >10 and 100 Hz.

For each range we calculate an average σ″ value from at least three frequencies ($\overline{\sigma}''_{LF}$, $\overline{\sigma}''_{MF}$, $\overline{\sigma}''_{HF}$). In a next step, we compute the relative differences d_{ML} between MF and LF, normalized to the mean value:

$$d_{ML} = 2\frac{\overline{\sigma}''_{MF} - \overline{\sigma}''_{LF}}{\overline{\sigma}''_{MF} + \overline{\sigma}''_{LF}}, \tag{3}$$

as well as the normalized relative difference d_{HM} between HF and MF as

$$d_{HM} = 2\frac{\overline{\sigma}''_{HF} - \overline{\sigma}''_{MF}}{\overline{\sigma}''_{HF} + \overline{\sigma}''_{MF}}. \tag{4}$$

We assign five different types by considering the differences d_{ML} and d_{HM}:

- **Type 1** – **ascending type**: increasing σ″ with increasing frequency ($d_{ML} > 0$ and $d_{HM} > 0$),
- **Type 2** – **descending type**: decreasing σ″ with increasing frequency ($d_{ML} < 0$ and $d_{HM} < 0$),
- **Type 3** – **constant type**: constant σ″ over all frequencies with an average deviation in d_{ML} and d_{HM} smaller than 10% ($\sqrt{|d_{ML} \times d_{HM}|} < 0.1$),
- **Type 4** – **maximum type**: maximum σ″ in the frequency interval between 1 and 10 Hz ($d_{ML} > 0$ and $d_{HM} < 0$),
- **Type 5** – **minimum type**: minimum σ″ in the frequency interval between 1 and 10 Hz ($d_{ML} < 0$ and $d_{HM} > 0$).

A sketch of the types is shown in Fig. 3b.

3. Results

3.1. Laboratory data

The laboratory IP spectra for all samples are shown in Fig. 4, presenting the conductivity in real σ′ (a, c, e, g) and imaginary part σ″ (b, d, f, h) in the frequency range between 10^{-3} and 10^{3} Hz. Due to high number of spectra, the samples from the Kanstein dump can be found in a) and b), the samples from the other slag dumps in c) and d). The ore sample spectra are shown and in e) and f), the spectra from the country rock samples are shown in g) and h).

Most of the slag samples from Kanstein show a similar range of conductivities, only sample SK 2 is characterized by higher values in both, real and imaginary part. Whereas for all samples the real part σ′ is always increasing to higher frequencies, the shape of the curve for σ″ varies. With increasing frequencies, we can distinguish visually between curves with an increasing σ″ (ascending type, KS 5, KS 6, KS 9), with a decreasing σ″ (descending type, KS 8), with a constant σ″ (constant type, SK 1) and with a maximum σ″ at medium frequencies (maximum type, SK 2).

The samples from the other slag dumps in the Harz Mountains show similar variation (Fig. 4c and d) in both real and imaginary part of conductivity. Again, the real part is always increasing with rising frequencies. The IP spectra for the ore (e, f) and country rock samples (g, h) can be also seen in Fig. 4. Both types of samples differ significantly. The ore samples show much higher values in both real and imaginary conductivity than the samples from the country rock. In addition to the four already mentioned types, the fifth type of curve shape is found for (e.g.) the claystone sample IFG-B12 that indicates a minimum of σ″ at medium frequencies (minimum type).

Besides the varying shapes of the σ″ spectra, another differentiation of the slags, which considers the levels of polarization magnitude, should be addressed. Similar to the metal factor used in ore prospection, the magnitude of polarization σ″ can be attributed to the amount of electronically conducting minerals (ore minerals) in the slag. The samples XS-03-1 and XS-05-1 show very low σ″ (10^{-4}–10^{-1} mS/m) whereas the values of the samples SO and XS-41 are up to six orders of magnitude higher (10^{2}–10^{3} mS/m). Most of the slag samples from all dumps are in a σ″ range between 0.5 mS/m and 10 mS/m. Considering the average σ″ value for the medium-frequency range ($\overline{\sigma}''_{MF}$), we assigned the samples into the three categories: low-, medium-, and high-grade slags. We defined samples with $\overline{\sigma}''_{MF} \leq 0.1$ mS/m as low-grade, 0.1 mS/m $< \overline{\sigma}''_{MF} <$ 1 mS/m as medium-grade and $\overline{\sigma}''_{MF} \geq 1$ mS/m as high-grade samples (see Table 3 and Fig. 4).

As expected, all pure ore samples are characterized by high-grade that indicates high metal content. The slag samples vary in their

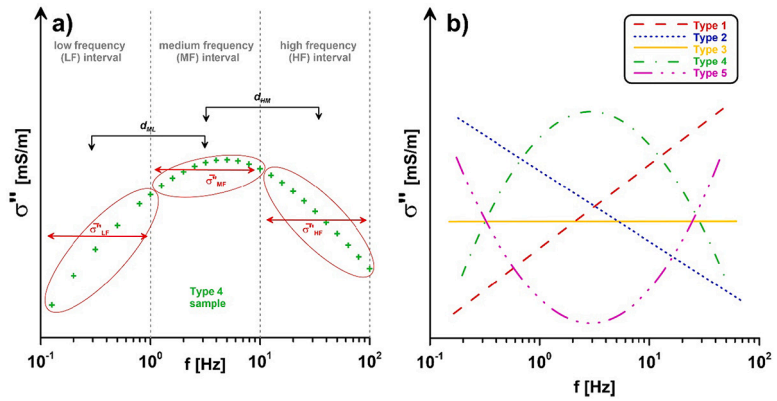

Fig. 3. Sketch of the calculation (a) and the classification (b) of the different spectral types.

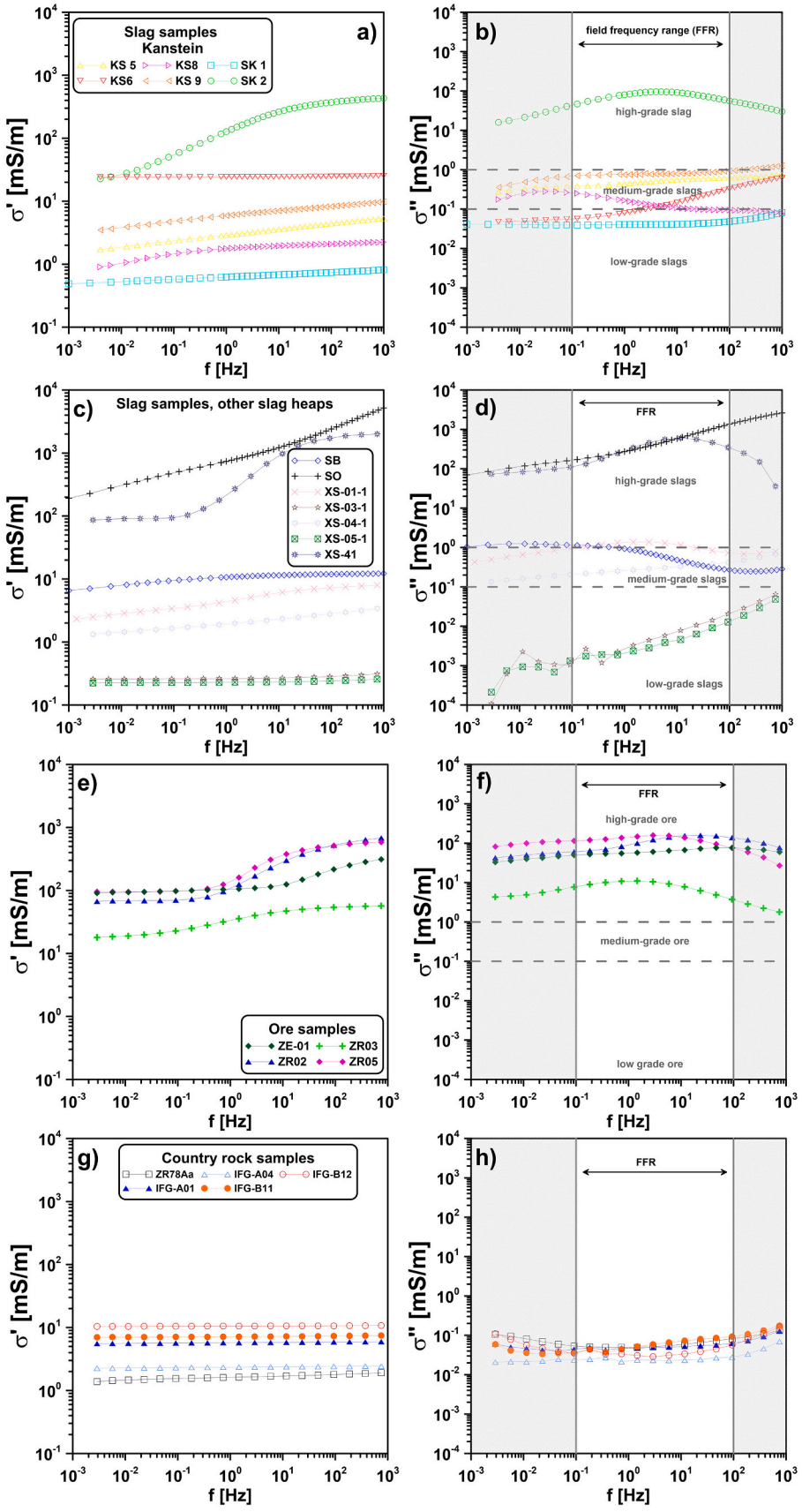

Fig. 4. Complex conductivity spectra in real part (a, c, e, g) and imaginary part (b, d, f, h) are shown for all slag samples at the Kanstein dump (a, b) and other slag dumps in the Harz Mountains (c, d). The results for the ore samples can be seen in e) and f), for the country rock samples in g) and h). FFR denotes the frequency range used in the field. Horizontal dashed lines represent the limits for the distinction in different slag/ore grades.

Table 3
Measured and calculated SIP values for all investigated samples.

Material	Name	σ' @ 0.1 Hz [mS/m]	σ' @ 100 Hz [mS/m]	Chargeability m [−]	$\overline{\sigma}'_{MF}$ [mS/m]	Ore/slag grade	Classification type
Slag	**XS-41**	93.51	1719	0.95	455.0	high	1
	SO	505.2	2403	0.79	416.1	high	1
	SK 2	59.26	371	0.92	91.71	high	4
	XS-01-1	3.39	7.22	0.53	1.349	high	4
	KS 9	4.93	8.28	0.41	0.779	medium	3
	SB	9.62	11.9	0.19	0.681	medium	2
	KS 5	2.41	4.42	0.46	0.506	medium	1
	XS-04-1	1.65	2.79	0.41	0.287	medium	1
	KS 8	1.50	2.09	0.28	0.130	medium	2
	KS 6	24.12	24.63	0.02	0.110	medium	1
	SK 1	0.58	0.74	0.21	0.041	low	3
	XS-03-1	0.26	0.28	0.08	0.004	low	1
	XS-05-1	0.23	0.24	0.06	0.003	low	1
Ore	**ZR05**	99.77	515.3	0.81	153.5	high	4
	ZR02	72.74	522.4	0.87	121.7	high	1
	ZR01	66.76	311.5	0.78	77.24	high	1
	ZE-01	97.96	216.2	0.55	60.68	high	1
	ZR03	25.13	53.92	0.58	10.27	high	4
Country rock	**ZR78A**	1.57	1.79	0.13	0.052	–	1
	IFG-A01	5.67	5.88	0.04	0.049	–	3
	IFG-A04	2.31	2.41	0.04	0.023	–	3
	IFG-A07	3.13	3.26	0.04	0.028	–	1
	IFG-B07	10.19	10.25	0.01	0.015	–	1
	IFG-B11	7.07	7.32	0.03	0.059	–	1
	IFG-B12	10.48	10.63	0.01	0.030	–	5

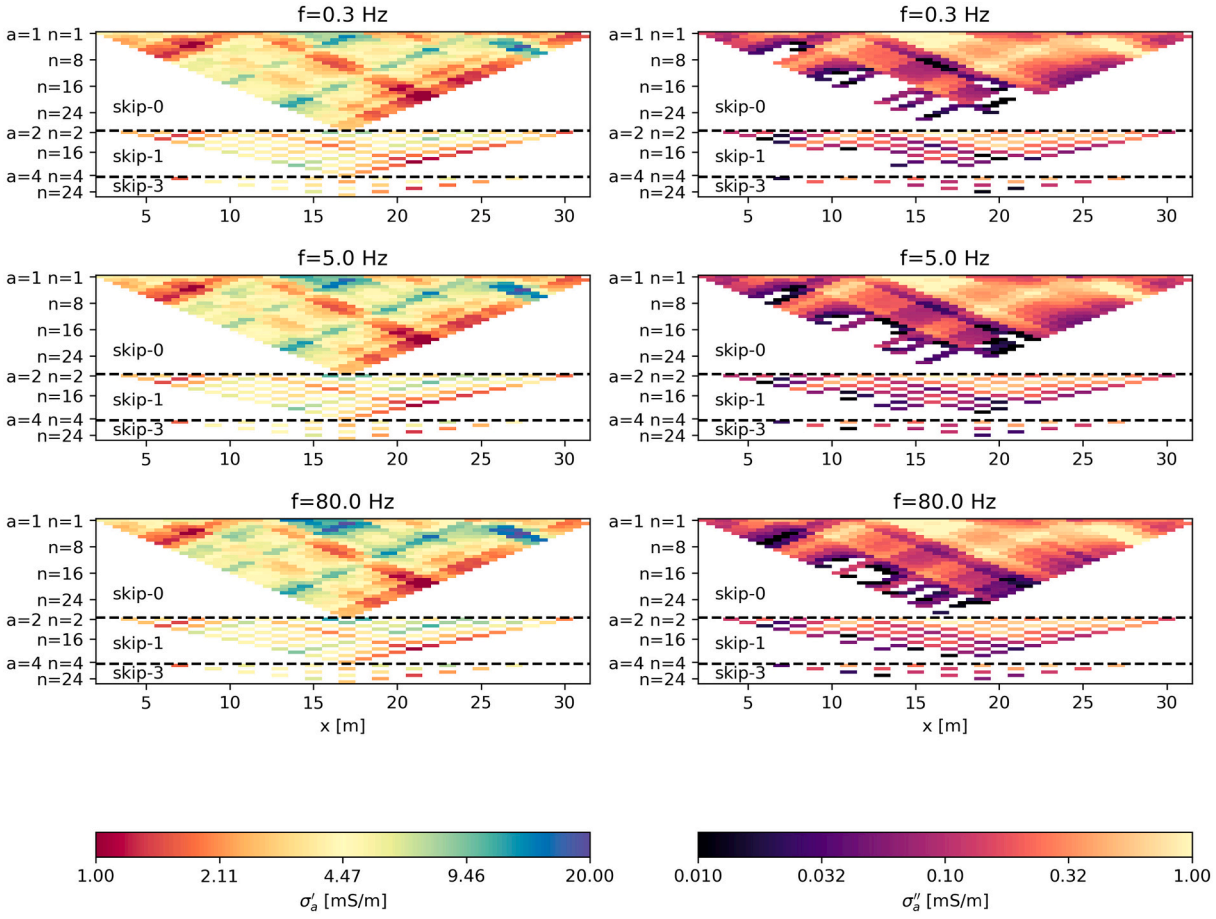

Fig. 5. Real (left) and imaginary (right) apparent conductivity for three different frequencies at Profile 1. First row: 0.3 Hz, middle row: 5 Hz and bottom row: 80 Hz. Missing data (white areas) in the imaginary conductivity indicate negative values. The different dipole lengths a = 1, 2, 4, (also denoted as skip-0, skip-1 and skip-3) are displayed one below the other (separated by the black dashed line). The respective n-values denote the different pseudo depths.

grade. Most of the slag samples are attributed to the high- or medium-grade range. The three more siliceous samples (SK 1, XS-03-1 and XS-05-1) with lower polarization are characterized as low-grade slag.

In a next step, we differentiate our samples according to our spectral classification (see above and Table 3). Obviously, most of the ore samples indicate a type 1 and type 4 behaviour in the FFR. These types can be found for the high-grade slags, too. Furthermore, type 2 and 3 slags could be found. Even though, several of the country rocks could be characterized by a type 5 over the entire laboratory frequency range, the country rocks are mainly classified as type 1 in the FFR.

3.2. Field data acquisition and inversion

The pseudo section for Profile 1, presented as σ' and σ'' for the three frequencies f = 0.3 Hz, 5 Hz and 80 Hz are shown in Fig. 5. We used three different dipole lengths (a = 1, 2, 4, also denoted as skip-0, skip-1 and skip-3) which are displayed one below the other (separated by the black dashed line). The respective n-values denote the different pseudo depths. The three σ' pseudo sections (to the left) are very similar and show irregular images with some diagonal traces corresponding to current or potential dipole groups. The range of the apparent σ' are mostly between 1 mS/m and 20 mS/m, whereas the apparent σ'' varies mostly between 0.01 mS/m and 1 mS/m with some removed data points with negative values on the bottom left side of the profile (white areas). Here, a general differentiation in zones with low polarization (left) and higher polarization (from the middle to the right) with maximal values on top is observed. Furthermore, high conductive areas (blue spots in σ') correlate with high polarization values in σ'' (yellow spots) and vice versa. Differences between the frequency ranges are hardly visible and are mainly caused by the increasing number of negative σ'' values at lower frequencies (which are masked with white colours).

In accordance with our laboratory classification system, we subdivided the resulting spectra in the above-mentioned three frequency ranges (LF: low-frequency, MF: medium-frequency and HF: high-frequency). The inversion results for three ranges (σ'_MF (left side) plus σ''_LF, σ''_MF and σ''_HF (to the right)) are presented in Fig. 6. The relative root mean square (rrms) errors for the inversion results are satisfying considering the large dynamic of the data (rrms(σ'_MF) = 10.6%, rrms(σ''_LF) = 31.9%, rrms(σ''_MF) = 16.2%, rrms(σ''_HF) = 12.9%).

Due to the low variability, the real conductivity σ' for the medium-frequency range (σ'_MF) is representative for all ranges. Here, we find mostly low conductivities (< 5 mS/m) with a layer of higher values (> 10 mS/m) on the right side of the profile and between 192 m and 194 m altitude. Note that we used a coverage threshold to cut away model cells that are not well covered. As Ronczka et al. (2017) demonstrate on a synthetic model, the coverage (sum of absolute sensitivity values over all data points normalized by the cell size) is a reasonable approximation for the model resolution. Similar to them, we use a threshold of 1 to make sure that only well-resolved model cells are shown.

In the σ'' sections (right side), an approx. 2–3 m thick layer of higher values (up to >1 mS/m) can be found near the surface in the middle and the right part of the profile. This layer is surrounded by areas with lower σ'' values and mainly corresponds with the high-conductive layer in the σ'-section.

Based on our laboratory results, we interpret that layer as high-grade slag material, whereas the surrounding areas might be attributed to medium- or low-grade slag or country rock material. Furthermore, it should be noted that no significant differences between the three frequency ranges are visible.

3.3. Evaluation of slag grade

To assign the slag grades of the profiles, we used the $\overline{\sigma}''_{MF}$ value for each cell of the subsurface. Fig. 7 displays the resulting depth section for Profile 1. We find areas with medium- and high-grade slags far to the left and as near-surface layer to the right. Large parts of the subsurface are assigned to low-grade material, which can be interpreted as low-grade

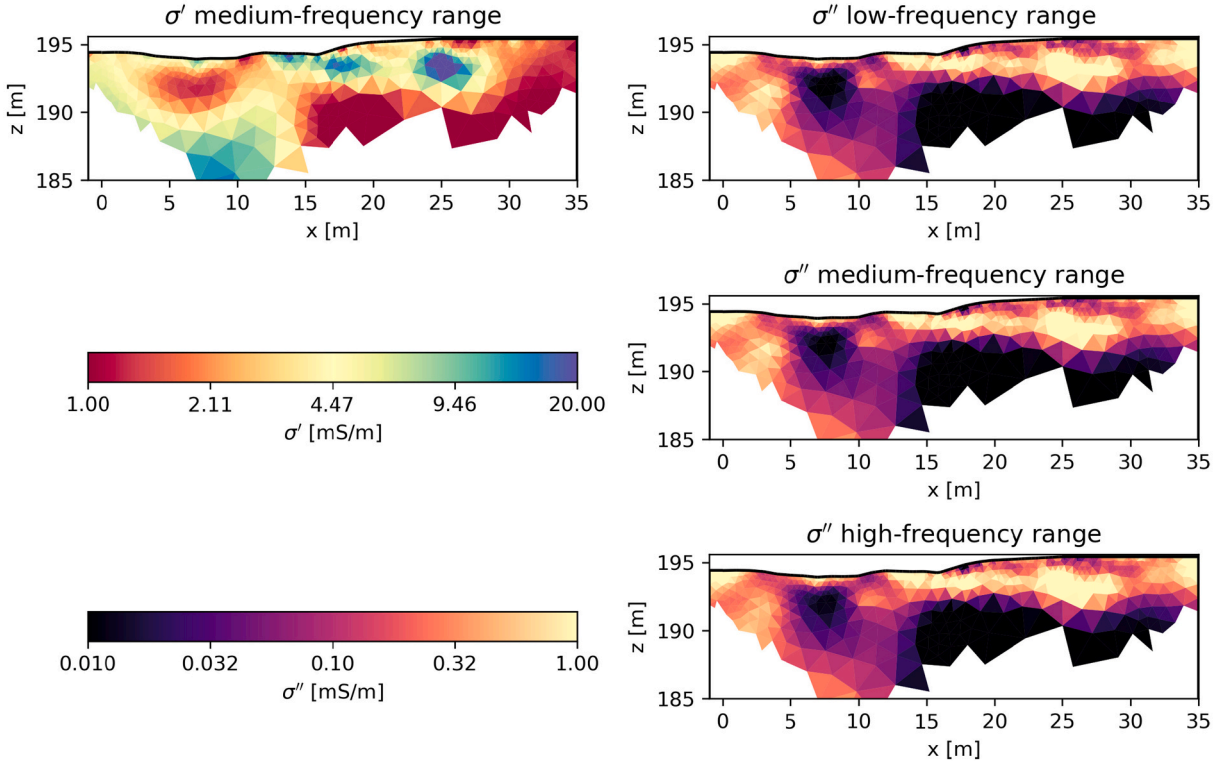

Fig. 6. Inversion results for Profile 1, assigned to the three frequency ranges low-frequency, medium-frequency, and high-frequency range. Left: σ' for the medium-frequency range, right: σ'' for the low-frequency (top), medium-frequency (middle) and high-frequency (bottom) range.

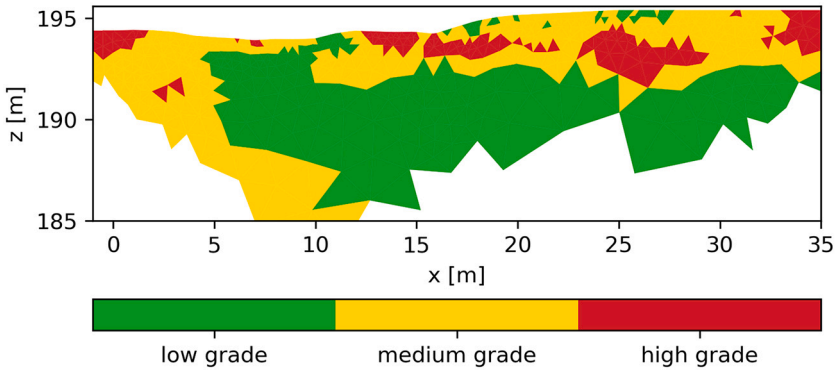

Fig. 7. Slag grades distribution for Profile 1.

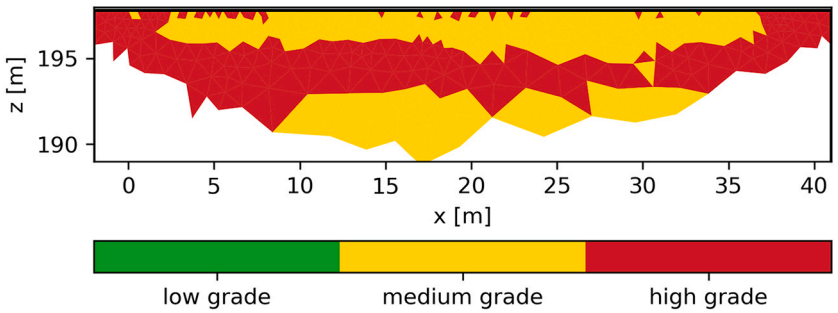

Fig. 8. Slag grade distribution for Profile 2, based on the SIP data previously published in Günther and Martin (2016).

slag or country rock.

The grade assignment was also done for Profile 2. The pseudo section and the inverted cross-section can be found in Günther and Martin (2016). Fig. 8 displays for the depth section of Profile 2 only medium- and high-grade slags. The high-grade slag material forms a more or less continuous horizontal layer between 193 m and 195 m altitude.

3.4. Classification of slag material

The application of the proposed classification with five spectral types to the resulting spectra for each cell of the subsurface enables a discrimination of the subsurface material according to the spectral behaviour.

Fig. 9 displays a depth section of the type classification for Profile 1. An extended type 1 area (red) is found in the left part of the profile for altitudes between approx. 190 m and 193 m. This spectral behaviour corresponds to the medium-grade slag samples KS 5 and KS 6 originating from the slag dump Kanstein. The depth section of the profile reveals some small to medium size type 2 areas (blue, e.g., to the far left and right). Type 2 spectra have been recorded for the slag material KS 8. The larger areas shown in yellow colour indicate type 3 spectra, which may reflect the deposition of slag material similar to the sample KS 9. Smaller spots of type 5 (purple) spectra demonstrate the resulting variability of the spectral behaviour. Areas with no colour are masked due to either a bad coverage or by not passing the threshold σ'' value of 0.1 mS/m, which is regarded as the lower limit of the medium-grade slags for which a spectral classification can be done.

The resulting classification image for Profile 2 shows various coherent layers of different types (Fig. 10). Below the top layer, there is a polarizable unit, which is characterized by type 1 spectra. We observe below the top type 1 layer another layer that is dominated by type 4 spectra, which we identify for the slag sample SK 2 originating from this

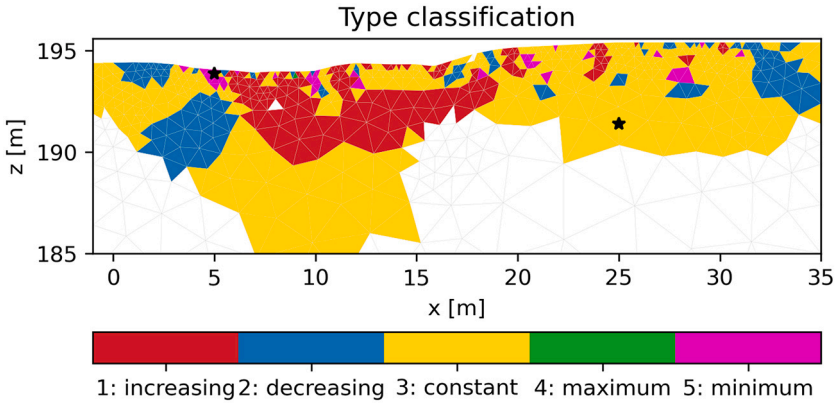

Fig. 9. Type classification for Profile 1. The two black stars represent selected positions for the types 3 and 5 used for the comparison between field and laboratory spectra (see Fig. 11). Areas with white colour are masked due to either a bad coverage or by not passing the threshold σ'' value of 0.1 mS/m.

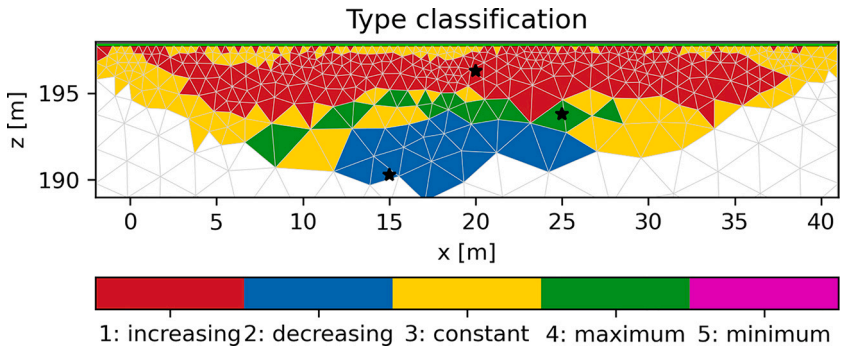

Fig. 10. Type classification for Profile 2 based on the SIP data previously published in Günther and Martin (2016). The three black stars represent selected position for the types 1, 2 and 4 and are used for the comparison between field and laboratory spectra (see Fig. 11). Areas with white colour are masked due to either a bad coverage or by not passing the threshold σ″ value of 0.1 mS/m.

slag dump. The extended type 2 structure at greater depth can be attributed to the spectral behaviour of the sample KS 8. However, due to the anisotropy caused by the layered structure, the depths of all layers might be overestimated during the inversion process.

4. Discussion

Based on our SIP investigations in the laboratory, we observed that slag samples show a wide variability in both polarization magnitude and spectral behaviour.

We could observe that the different slag samples show varying polarization magnitudes and thus different ore grades. This grading classification can then be used as an additional factor to estimate the value of the slag as re-usable raw material.

From the classification system based on the spectral behaviour of σ″, similarities between the different samples could be observed. In general, the slag material could be characterized by one of the first four types (ascending, descending, constant, maximum) whereas the minimum type was found for the country rock material. In analogy to the ore samples, most of the slag samples are characterized as type 1 or 4.

This finding is in good accordance with SIP results published by other authors (Campbell, 2001; Florsch et al., 2011; Qi et al., 2018). Most of the slag samples presented by Qi et al. (2018) indicate a maximum type 4, whereas Campbell (2001) also reported the ascending type 1 (for the phase shift).

The classification images from the field profiles (Figs. 9 and 10) clearly demonstrate the diversity of the dumped slag material. The resulting images also reflect the long and diverse history of this dump with the staggered fillings at different operating periods.

We picked selected spectra from the field sections (black stars in Figs. 9 and 10, see also Table 4), representing only the different types but not real samples at these locations, and compared them with the types from the laboratory samples at the same slag dump. Fig. 11 displays the spectra retrieved from the multi-frequency IP field measurements as filled symbols and the laboratory samples as open symbols. Even though the laboratory samples were taken from the same dump, they could only be picked from the surface from different spots over the entire dump, which results in natural differences due to the inhomogeneity of the dump.

Table 4
Overview of the position for the different types in the field measurements (black stars in Figs. 9 and 10).

Classification type	Profile	Coordinates [m] (x/z)	Seen in
1	2	20/196	Fig. 10
2	2	15/190.4	Fig. 10
3	1	25/191.4	Fig. 9
4	2	25/193.5	Fig. 10
5	1	5/193.9	Fig. 9

Considering the very good data quality for Profile 2, we extend the frequency range of the field spectra to 500 Hz. Obviously, the real part of conductivity (σ′, Fig. 11a) of the inverted spectra retrieved from the field measurements indicate a much smaller variation (2–20 mS/m) in comparison with the measured spectra in the laboratory (0.5–500 mS/m). Possibly, the salinity of the fluid and the saturation of the samples during the laboratory measurements does not correspond to the in-situ values in the slag dump. We observed a permanent increase of water conductivity during the storage of the samples in the containers. This is caused by partial dissolution of slag material during the long-time storage. Up to now, our laboratory experiments have not been able to simulate the temporal changes of water conductivity and saturation in the slag material of the dump. Assuming that water conductivity and saturation affect the spectral behaviour less than the absolute values of σ′ and σ″, we focus the comparison on the spectral behaviour.

The principal shapes of the σ″ spectra (Fig. 11b) are comparable for each type from both the field and laboratory results, even though differences in the magnitude can be observed. In particular, the type 4 laboratory spectrum differs remarkably, whereas both type 2 samples show similar values. Nevertheless, both type 4 spectra are characterized by the highest conductivities whereas the type 3 spectra show the respective lowest conductivities.

The difference in the spectra can be also explained by the regarded volume. The laboratory measurement of the high-grade sample SK 2 considers only a volume of a few cubic centimetres. The field measurement integrates over a much bigger volume that might represent a mixture of high-grade slag with low-grade material that causes a decrease in both σ′ and σ″. Furthermore, the unconsolidated samples reflect the dump site conditions better due to the higher variability in the material composition (e.g., a wide grain size distribution) in contrast to the small solid sample (e.g., SK 2) where the material can be quite random.

Campbell (2001) reported that the SIP data measured in the laboratory do not correspond very well with the SIP data measured in the field for several mine dumps. Due to the above-mentioned reasons, a direct comparison will be often very difficult or even delusive. Instead, a comparison of the spectral shape seems to be a more realistic and promising approach.

Our slag classification system is based on two thresholds. First, we only take spectra into account with a polarization magnitude of $\sigma'' > 0.1$ mS/m and second, the deviation from the constant type (3) over all frequencies is defined by a relative deviation up to 10% (eqs. 5 and 6). By changing these thresholds, slightly varying results have been obtained, which, from our prospective, seemed to be less realistic and therewith harder to explain. However, depending on the investigation aim and the characteristic of the dump, these parameters might be modified for other locations.

The here presented classification can be used as a tool to discriminate

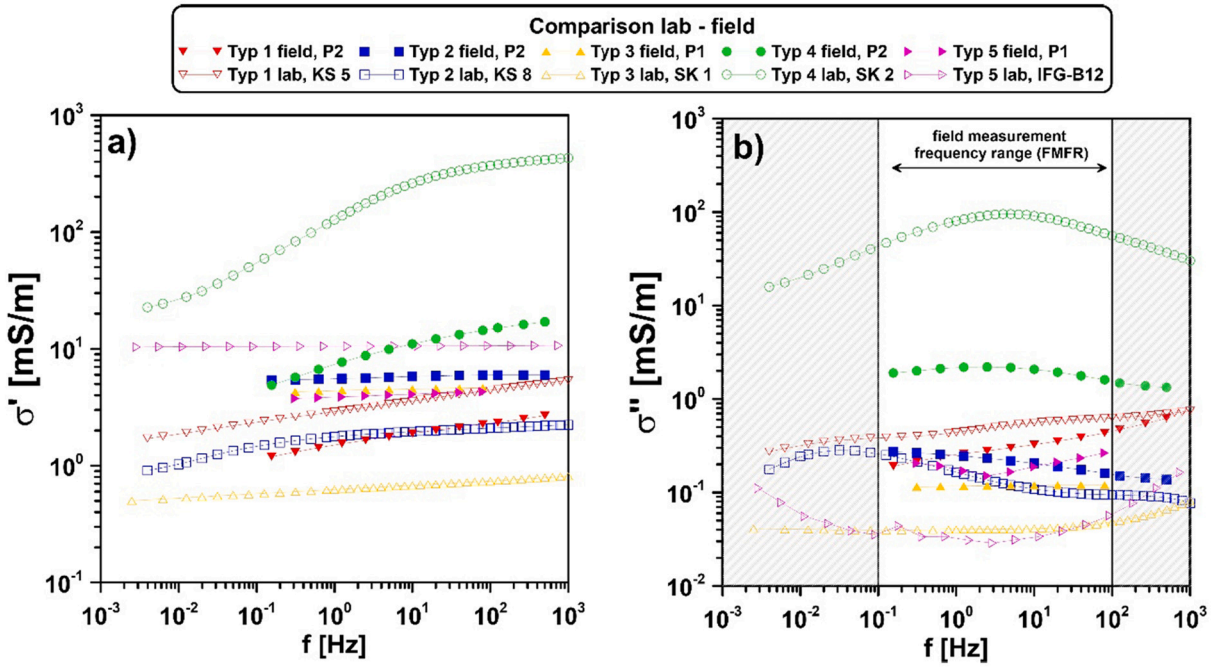

Fig. 11. Comparison of the spectral types between laboratory and field SIP spectra from slag dump Kanstein samples. a) Real part of conductivity σ′, b) imaginary part of conductivity σ″. The origin of the samples are marked by P1/P2 (Profiles 1 and 2 according to the black starts in Figs. 9 and 10, see also Table 4) as well as by the sample name of the laboratory measurements (e.g., KS 5).

between different kind of slags and the surrounding material based on their polarization behaviour in a broad frequency range. In contrast to IP measurements measured at only one frequency (e.g., 1 Hz in frequency-domain) or by just considering the total chargeability (in time-domain), the classification into different types (Figs. 9 and 10) offers additional information compared with only the slag grade sections (Figs. 7 and 8). Therefore, a discrimination between different types of slags, which have been deposited over the years, seems to be possible.

In general, our samples demonstrate the diversity of the spectral behaviour of slag material. The proposed classification can be independently used for all types of polarization curves without fitting to any predefined model (e.g., Cole-Cole, Generalized Cole-Cole, Cole-Davidson, Constant Phase Angle). Therefore, it enables a suitable comparison between materials measured in the laboratory and in the field in general.

By measuring SIP in the field with a 3D survey (or with sufficiently dense 2D lines), it is even possible to estimate the volume of a special type of slag following the procedure of slag volume estimation presented by Martin et al. (2020b). Therewith, an assessment of the amount or the value of the residuals in an economic context might be possible if the metal content of the different slag types can be retrieved.

5. Conclusions

The SIP method can be used to investigate the potential economic value of historical slag dumps and to estimate the environmental impact due to contamination. By measuring over a broad frequency range, a classification of the different slag types as well as a discrimination between valuable material and surrounding country rock proved to be possible. The spectral classification into five types, depending on the shape of the σ″ spectrum, provides additional information about the subsurface and the diversity of slags. This classification was restricted to the field frequency range (0.1 Hz – 100 Hz). The different types were first attributed to the laboratory spectra and subsequently to the spectra retrieved from two field SIP profiles at the same slag dump. The comparison between laboratory and field spectra confirmed the diversity of the spectral behaviour of slag material. Differences in saturation, fluid conductivity, and the regarded volume in the laboratory and field experiments might explain the variation of measured magnitudes in both real and imaginary conductivity. A transferability between laboratory and field spectra based on the classification types is promising but needs further investigation and verification at a wider database. However, the proposed method can provide the basis for assessing the value of reusable material in slag dumps.

Declaration of Competing Interest

The authors declare that they have no known competing financial interests or personal relationships that could have appeared to influence the work reported in this paper.

Acknowledgment

The work was funded by the German Ministry of Education and Research (BMBF) due to the project ROBEHA (grant 033R105). We acknowledge the help from the BGR colleagues Ursula Noell, Rudolf Knieß, Claudia Wießner, Manfred Ratz, Ralf Seibold and Matthias Sack during field work.

Appendix A. Supplementary data

Supplementary data to this article can be found online at https://doi.org/10.1016/j.jappgeo.2021.104439.

References

Börner, F.D., Schopper, J.R., Weller, A., 1996. Evaluation of transport and storage properties in the soil and groundwater zone from induced polarization measurements. Geophys. Prospect. 44, 583–601.
Campbell, D.L., 2001. Spectral Induced polarization measurements at the Main Iron Incline Mine Dump near Leadville, Colorado. USGS Rep. 01-315.
Cole, K.S., Cole, R.H., 1941. Dispersion and adsorption in dielectrics. I. Alternating current characteristics. J. Chem. Phys. 9, 341–351.
Denecke, D., 1978. Erzgewinnung und Hüttenbetriebe des Mittelalters im Oberharz und im Harzvorland (Mining and melting during the Middle Ages in the Upper Harz and in the Harz region). Archäolog. Korrespondenzbl. 8, 77–86 (in German).
Dissado, L., Hill, R.M., 1984. Anomalous low-frequency dispersion. J. Chem. Soc. Faraday Trans. 80, 291–319.

Fiandaca, G., Auken, E., Gazoty, A., Christiansen, A.V., 2012. Time-domain induced polarization: full-decay forward modeling and 1D laterally constrained inversion of Cole–Cole parameters. Geophysics 77, E213–E225.
Florsch, N., Llubes, M., Tereygeol, F., Ghorbani, A., Roblet, P., 2011. Quantification of slag heap volumes and masses through the use of induced polarization: application to the Castel-Minier site. J. Archaeol. Sci. 38, 438–451.
Florsch, N., Llubes, M., Tereygeol, F., 2012. Induced polarization 3D tomography of an archaeological direct reduction slag heap. Near Surf. Geophys. 10, 567–574.
Florsch, N., Feras, A., Bonnenfant, J., Camerlynck, C., 2017. La polarisation provoque, outil geophysique de spatialisation des amas de scories pour lestimation des productions sidrurgiques - induced polarization: a geophysical tool for slag characterization and ancient iron production assessment. ArcheoScience 41-2, 23–33 (in French).
Günther, T., Martin, T., 2016. Spectral two-dimensional inversion of frequency-domain induced polarisation data from a historical mining slag heap. J. Appl. Geophys. 135 https://doi.org/10.1016/j.jappgeo.2016.01.008.
Günther, T., Rücker, C., Spitzer, K., 2006. 3-d modeling and inversion of DC resistivity data incorporating topography - Part II: Inversion. Geophys. J. Int. 166, 506–517.
Hupfer, S., Martin, T., Weller, A., Günther, T., Kuhn, K., Ngninjioc, V.D.N., Noell, U., 2016. Polarization effects of unconsolidated sulphide-sand-mixtures. J. Appl. Geophys. 135 https://doi.org/10.1016/j.jappgeo.2015.12.003.
Johansson, S., Lindskog, A., Fiandaca, G., Dahlin, T., 2020. Spectral induced polarization of limestone: time domain field data, frequency domain laboratory data and physicochemical rock properties. Geophys. J. Int. 220, 928–950. https://doi.org/10.1093/gji/ggz504.
Kruschwitz, S., 2007. Assessment of the Complex Resistivity Behavior of Salt Affected Building Materials. PhD thesis. TU Berlin, Germany.
Kuhn, K., Meima, J.A., 2019. Characterization and economic potential of historic tailings from gravity separation: Implications from a mine waste dump (Pb-Ag) in the Harz Mountains mining district, Germany. Minerals 9, 303.
Kuhn, K., Goldmann, S., Goldmann, D., Qiu, H., Rammlmair, D., 2021. The distribution of metals into primary and secondary phases in historical lead-silver smelting slags from Rammelsberg ore deposit and implications for their recovery. J. Geochem. Explor.
Lesmes, D.P., Frye, K.M., 2001. The influence of pore fluid chemistry on the complex conductivity and induced-polarization responses of Berea sandstone. J. Geophys. Res. 106, 4079–4090.
Liessmann, W., 2010. Historischer Bergbau im Harz. Springer, Berlin/Heidelberg, Germany, p. 470.
Loke, M.H., Chambers, J.E., Ogilvy, R.D., 2006. Inversion of 2D spectral induced polarization imaging data. Geophys. Prospect. 54, 287–301.
Martin, T., Günther, T., Flores Orozco, A., Dahlin, T., 2020a. Evaluation of spectral induced polarization field measurements in time and frequency domain. J. Appl. Geophys. 180 https://doi.org/10.1016/j.jappgeo.2020.104141.
Martin, T., Kuhn, K., Günther, T., Kniess, R., 2020b. Geophysical exploration of a historical stamp mill dump for the volume estimation of valuable residues. J. Environ. Eng. Geophys. 25, 275–286. https://doi.org/10.2113/JEEG19-080.
Nordsiek, S., Weller, A., 2008. A new approach to fitting induced-polarization spectra. Geophysics 73 (6), F235–F245.
OpenTopoMap, 2021. https://opentopomap.org/#map=11/51.7695/10.5290.
Pelton, W.H., Ward, S.H., Hallof, P.G., Sill, W.R., Nelson, P.H., 1978. Mineral discrimination and removal of inductive coupling with multifrequency IP. Geophysics 43, 588–609.
Pelton, W.H., Sill, W.R., Smith, B.D., 1983. Interpretation of complex resistivity and dielectric data — part 1. Geophys. Trans. 29, 297–330.
Placencia-Gomez, E., Parviainen, A., Hokkanen, T., Loukola-Ruskeeniemi, K., 2010. Integrated geophysical and geochemical study on AMD generation at the Haveri Au-Cu mine tailings, SW Finland. Environ. Earth Sci. 61, 1435–1447.
Placencia-Gomez, E., Slater, L., Ntarlagiannis, D., Binley, A., 2013. Laboratory SIP signatures associated with oxidation of disseminated metal sulfides. J. Contam. Hydrol. 148, 25–38.
Placencia-Gomez, E., Parviainen, A., Slater, L., Leveinen, J., 2015. Spectral induced polarization (SIP) response of mine tailings. J. Contam. Hydrol. 173, 8–24.
Qi, Y., Ahmed, A.S., Revil, A., Ghorbani, A., Abdulsamad, F., Florsch, N., Bonnenfant, J., 2018. Induced polarization response of porous media with metallic particles part 7: Detection and quantification of buried slag heaps. Geophysics 83, E277–E291.
Ronczka, M., Hellman, K., Günther, T., Wisen, R., Dahlin, T., 2017. Electric resistivity and seismic refraction tomography, a challenging joint underwater survey at Aspö hard rock laboratory. Solid Earth 8, 671–682. https://doi.org/10.5194/se-8-671-2017.
Rücker, C., Günther, T., Spitzer, K., 2006. 3-d modeling and inversion of DC resistivity data incorporating topography - part I: Modeling. Geophys. J. Int. 166, 495–505.
Schleifer, N., Weller, A., Schneider, S., Junge, A., 2002. Investigation of a Bronze Age plankway by spectral induced polarisation. Archaeol. Prospect. 9, 243–253.
Sperling, H., Stoppel, D., Dennert, H., Tiemann, K.-Chr., 1981. Die Blei-Zink-Erzgänge des Oberharzes - Gangkarte des Oberharzes mit Erläuterungen. Geologisches Jahrbuch - Monographien der deutschen Blei-Zink-Erzlagerstätten 3, band D 46, p. 90. ISBN 978-3-510-96146-7.
Stedingk, K., Stoppel, D., 1993. Stratigraphy, petrography, petrogenesis, and tectonic features of the Upper and Middle Harz vein districts. In: Möller P., Lüders V. (eds): Formation of hydrothermal vein deposits. A case study of the Pb-Zn, barite and fluorite deposits of the Harz Mountains. Monogr. Ser. Mineral Dep. 30, 35–54.
Tarasov, A., Titov, K., 2013. On the use of the cole-cole equations in spectral induced polarization. Geophys. J. Int. 195, 352–356.
Ullrich, B., Weller, A., Günther, T., Rücker, C., 2007. Geophysical prospecting of ancient slag deposits in Munigua (Spain) and Ain-al Hajer (Morocco) using complex resistivity tomography. In: Presented at the 2nd International Conference Archaeometallurgy in Europe.
Weller, A., Brune, S., Hennig, T., Kansy, A., 2000. Spectral induced polarization at a medieval smelting site. In: Proceedings of the 6th Meeting Environmental and Engineering Geophysics (EEGS-ES), Bochum, Germany: EL, p. 11.
Weller, A., Slater, L., Nordsiek, S., Ntarlagiannis, D., 2010. On the estimation of specific surface per unit pore volume from induced polarization: a robust empirical relation fits multiple datasets. Geophysics 75 (4), WA105–WA112.
Wikimedia, 2021. https://commons.wikimedia.org/wiki/File:Locator_map_of_Germany.svg.
Yoshioka, K., Zhdanov, M.S., 2005. Three-dimensional nonlinear regularized inversion of the induced polarization data based on the Cole–Cole model. Phys. Earth Planet. Inter. 150, 29–43.
Zimmermann, E., Kemna, A., Berwix, J., Glaas, W., Vereecken, H., 2008. EIT measurement system with high phase accuracy for the imaging of spectral induced polarization properties of soil and sediments. Meas. Sci. Technol. 19, 094010.